Atmospheric
Chemistry
and Physics
Discussions

Eddy flux measurements of sulfur dioxide deposition to the sea surface

Jack G. Porter[1], Warren De Bruyn[2], and Eric S. Saltzman[1]

[1]Department of Chemistry and Department of Earth System Science, University of California Irvine, Irvine, CA, USA
[2]Department of Chemistry and Biochemistry, Chapman University, Orange, CA, USA

Correspondence: Jack G. Porter (jgporter@uci.edu)

Abstract. Deposition to the sea surface is a major atmospheric loss pathway for many important trace gases, such as sulfur dioxide, (SO_2). The air/sea transfer of SO_2 is controlled entirely on the atmospheric side of the air/sea interface due to high effective solubility and other physical/chemical properties. There have been few direct field measurements of such fluxes due to the challenges associated with making fast response measurements of highly soluble trace gases at very low ambient levels.

5 In this study, we report direct eddy covariance air/sea flux measurements of SO_2, sensible heat, water vapor, and momentum. The measurements were made over shallow coastal waters from the Scripps Pier, La Jolla, CA using negative ion chemical ionization mass spectrometry as the SO_2 sensor. The observed transfer velocities for SO_2, sensible heat, water vapor, and momentum and their wind speed-dependences indicate that SO_2 fluxes can be reliably measured using this approach. As expected, the transfer velocities for SO_2, sensible heat, and water vapor are smaller than that for momentum, demonstrating

10 the contribution of molecular diffusion to the overall air-side resistance to gas transfer. Furthermore, transfer velocities of SO_2 were smaller than those of sensible heat and water vapor when observed simultaneously. This result is attributable to diffusive behavior in the interfacial layer of the air/sea interface.

Copyright statement.

1 Introduction

15 The deposition of soluble trace gases to the ocean surface is an important component in the global budgets of several important biogeochemical elements. For example, roughly 90 Tg y^{-1} of SO_2 are emitted to the atmosphere from fossil fuel combustion and industrial processes, from volcanic outgassing, and from the atmospheric photochemical oxidation of biogenic dimethyl-sulfide. In the marine atmosphere, SO_2 oxidation contributes to the production and growth of aerosols which influence the Earth's radiation budget via aerosol backscatter of solar radiation and cloud optical properties. Global models estimate that

20 dry deposition of SO_2 to the sea surface comprise slightly less than half of the total removal from the atmosphere (Sheng et al., 2015; Chin et al., 2000). The parameterization of dry deposition of soluble gases in atmospheric chemistry models is based largely on laboratory experiments, micrometeorological theory, or field studies in terrestrial environments (Liu et al.,

1979; Liss, 1973; Mackay and Yeun, 1983). Few direct flux studies of soluble trace gas deposition to the sea surface have been carried out due to the unavailability of chemical sensors with sufficient sensitivity and response time for eddy covariance flux measurements. Such studies are now feasible for SO_2 due to progress in the development of sensitive, fast response analytical methods (Thornton et al., 2002; Bandy et al., 2002). Bandy et al. (2002) developed a fast-response chemical ionization mass

5 spectrometer for aircraft measurement of SO_2 abundance and eddy covariance fluxes. Faloona et al. (2009) inferred air/sea surface fluxes from airborne eddy correlation measurements of SO_2 flux within the marine boundary layer. To our knowledge, there have been no prior studies of atmospheric SO_2 deposition involving eddy covariance in the marine surface layer. In this work we made eddy covariance flux measurements of SO_2 deposition to the coastal ocean from the Scripps Institute of Oceanography pier in La Jolla, California. These measurements were accompanied by simultaneous measurements of air/sea

10 fluxes of momentum, water vapor, and sensible heat. The goals of this study were: 1) to directly determine the transfer coefficient of SO_2 and its wind speed dependence for comparison to existing estimates, 2) to compare the transfer coefficients of SO_2 with those of momentum, water vapor, and sensible heat to assess the relative importance of turbulent and diffusive resistance to SO_2 deposition, and 3) to attempt to detect the dependence of soluble gas deposition on molecular diffusivity in the marine environment.

15 ## 2 Background

2.1 Air/sea gas transfer of highly soluble gases

Gas transfer across a gas liquid interface is commonly parameterized as follows:

$$F = K\left(C_a - \frac{C_w}{\alpha}\right) \tag{1}$$

Where F is the air/sea flux (mol m^{-2} s^{-1}), C_a and C_w are bulk air and water side concentrations (mol m^{-3}), and α is the

20 dimensionless solubility or Ostwald coefficient, C_w/C_a. K represents the bulk gas transfer coefficient reflecting the physical processes limiting exchange on both sides of the interface, expressed in air side units (m s^{-1}). The reciprocal of K, or resistance, can be partitioned into liquid side and air side processes, where:

$$K^{-1} = R_{total} = r_w + r_a = \frac{1}{k_w} + \frac{\alpha}{k_a} \tag{2}$$

In the case of gases like SO_2 with very high effective solubility ($\alpha \gg 1$) (Liss, 1971; Liss and G. Slater, 1974) and negligi-

25 ble seawater concentration (see below), the air side dominates the total resistance (i.e. $r_a \gg r_w$) so the gas transfer equation becomes:

$$F = k_a\left([SO_2]_a - \frac{[SO_2]_w}{\alpha}\right) \approx k_a[SO_2]_{air} \tag{3}$$

where k_a is the air side gas exchange coefficient (m s^{-1}), also referred to as the deposition velocity. The transfer coefficient, k_a (hereafter referred to as k_{SO2}) encapsulates the physical processes controlling transport across the marine atmospheric surface

30 layer to the air/sea interface. This transport is governed by: 1) turbulence in the surface layer, and 2) molecular diffusion close

to the sea surface where turbulence is suppressed by molecular viscosity (Liss and G. Slater, 1974; Slinn et al., 1978). The transfer coefficient can be expressed in terms of resistance to deposition, as follows:

$$k_a^{-1} = r_{total} = r_{turbulence} + r_{diffusion} \tag{4}$$

The turbulent resistance term, sometimes referred to as aerodynamic resistance, is often approximated by the momentum

5   transfer coefficient (or drag coefficient) under the assumption that there is no diffusive barrier to momentum transfer. Diffusive resistance is usually conceptualized in terms of the surface renewal model, involving periodic exchange of patches of near-surface air by turbulent eddies, with deposition of a trace gas to the sea surface via non-steady-state diffusion (Higbie, 1935; Danckwerts, 1951). This model implies a dependency on molecular diffusivity, as follows:

$$r_{diffusion} \propto Sc^n \tag{5}$$

10   where Sc is the Schmidt number defined as the kinematic viscosity of air (ν) divided by the molecular diffusion coefficient (D) of the gas in air and n is a constant.

2.2 Physical chemical properties of SO_2 relevant to gas transfer

The interpretation of the SO_2 air/sea flux measurements in this study are based on the following premises: 1) deposition of SO_2 is controlled entirely on the air side of the air/sea interface, and 2) surface ocean waters are always highly undersaturated

15   in SO_2 with respect to the overlying atmosphere. In this section we discuss the basis for these assumptions.

2.2.1 Effective solubility of SO_2 and the kinetics of ionic equilibria

Sulfur dioxide is not a highly soluble gas, but it has a very large effective solubility in aqueous solution at elevated pH because of the dissociation of aqueous SO_2 into bisulfite and sulfite ions (HSO_3^-; SO_3^{2-}). Collectively, dissolved SO_2 and its ionized forms are referred to as S(IV). The equilibria governing the aqueous speciation of SO_2 are listed below, with equilibrium

20   constants given for seawater at 298 K (Millero et al., 1989).

$$SO_2 \rightleftharpoons SO_{2aq} \qquad H_{SO2} = \frac{[SO_{2aq}]}{P_{SO2}} = 1.24 \, M \, atm^{-1} \tag{R1}$$

$$SO_2H_2O \rightleftharpoons HSO_3^- + H^+ \qquad K_1 = \frac{[HSO_3^-][H^+]}{[SO_2H_2O]} = 2.6 \times 10^{-2} \, M \tag{R2}$$

$$HSO_3^- \rightleftharpoons SO_3^{2-} + H^+ \qquad K_2 = \frac{[SO_3^{2-}][H^+]}{[HSO_3^-]} = 7.4 \times 10^{-7} \, M \tag{R3}$$
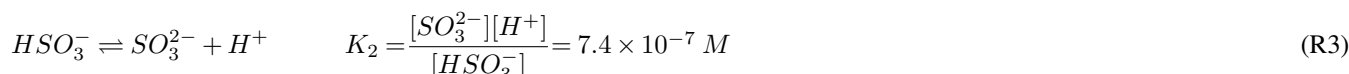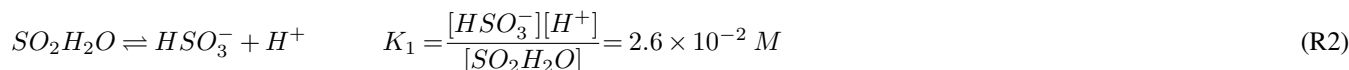
Combining these equilibria yields an effective SO_2 solubility, as follows:

25    $$H_{eff} = H_{SO2}\left[1 + \frac{K_1}{[H^+]} + \frac{K_1K_2}{[H^+]^2}\right] \tag{R4}$$

H_{SO2} is the Henry's law solubility (M atm^{-1}), K_1 and K_2 are equilibrium constants in reactions R2 and R3, R is the gas constant (L atm K^{-1} mol^{-1}) and T is temperature (K). At the pH of seawater, H_{eff} is 1×10^{-7} M atm^{-1}.

As noted by Liss (1971), the kinetics of S(IV) ionization in seawater are rapid, occurring on time scales much shorter than those for transport across the water side interfacial layer. Based on rate constants for the forward and reverse reactions

5   comprising the equilibria listed above, the characteristic time for equilibration of dissolved SO$_2$ with the ionic forms of S(IV) is roughly 4.5×10^{-4} s (Schwartz and Freiberg, 1981), while the time scale for diffusive transport through the interfacial layer on the water side is on the order of seconds (Hoover and Berkshire, 1969). Consequently, SO$_2$ behaves as a highly soluble gas during the air/sea exchange process.

The mass accommodation of SO$_2$ at the seawater surface is a potential source of resistance to air/sea gas transfer that was not

10   considered by Liss (1971). Laboratory studies of SO$_2$ uptake on water droplets show that the mass accommodation coefficient of SO$_2$ is about 0.1 (Worsnop et al., 1989). This is sufficiently large that the characteristic time for transport across the air/water interface is much smaller than that for transport to the water surface (Schwartz and Freiberg, 1981).

2.2.2   Placing a limit on the surface ocean concentration of S(IV)

To our knowledge, there are no published measurements of surface ocean S(IV). Here we place an upper limit on surface ocean

15   S(IV) based on rough estimates for the sources of S(IV) to the ocean, and the oxidation kinetics of S(IV) in seawater. The sources of S(IV) to the surface ocean include, 1) release of hydrogen sulphide (H$_2$S) from marine sediments or deep waters, followed by oxidation to S(IV), 2) atmospheric deposition of SO$_2$, 3) production of H$_2$S in surface waters from hydrolysis of photochemically-produced carbonyl sulfide (OCS) followed by oxidation, and 4) production of H$_2$S in surface waters from particulates and/or organisms. For the sediment source, we take the upper limit of about 10^{-1} mol m^{-2} y^{-1} from the global

20   compilation of sulfate reduction rates by Bowles et al. (2014). For the atmospheric source, an atmospheric SO$_2$ mixing ratio of 1 nmol mol^{-1} and a deposition velocity of 0.02 m s^{-1} yields a source of 2.6×10^{-3} mol m^{-2} y^{-1}. The other sources are many orders of magnitude smaller, based on surface ocean distributions and laboratory hydrolysis rates of OCS (Elliott et al., 1987; Cutter and Krahforst, 1988; Radford-Knoery and Cutter, 1994). Assuming that all of these sources are delivered to a shallow mixed layer of 10 m depth yields a upper limit on the S(IV) production rate (P$_{S(IV)}$) of about 10^{-2} mol m^{-3} y^{-1}. For the open

25   ocean, the S(IV) production rate is likely much lower, because the sulfide from sedimentary sulfate reduction is not released directly into the surface ocean. The kinetics of oxidation of S(IV) in seawater was measured in the laboratory by Zhang and Millero (1991). They report the following rate expression:

$$\frac{[S(IV)]}{dt} = k_{oxidation}[S(IV)]^2 \tag{6}$$

[S(IV)] is the seawater concentration of S(IV) (M) and k$_{oxidation}$ is the S(IV) oxidation rate constant (M^{-1} s^{-1}) with a value

30   of 1×10^4 M^{-1} min^{-1}. The steady state surface ocean S(IV) can be calculated as a balance between sources and oxidation, as follows:

$$P_{S(IV)} = k_{oxidation}[S(IV)]^2 \tag{7}$$

$$S(IV) = \sqrt{\frac{P_{S(IV)}}{k_{oxidation}}} \tag{8}$$

yielding a steady state S(IV) concentration of roughly 6×10^{-8} M. Based on the effective solubility of SO_2 in seawater, this represents an equilibrium SO_2 gas phase mixing ratio of only 2 fmol mol^{-1}. That is roughly three orders of magnitude lower than typical atmospheric SO_2 levels over the ocean (De Bruyn et al., 2006; Bandy et al., 1992; Chin et al., 2000). Therefore, one can justifiably assume that the sea surface is highly undersaturated in SO_2 with respect to the overlying atmosphere. It follows that the bulk air/sea concentration difference for SO_2 is essentially equal to the air side concentration (equation 3).

3 Methods

3.1 Study site and experimental setup

This study was conducted at Scripps pier located in La Jolla, California during April, 2014. The local meteorology is characterized by a daily westerly sea-breeze with occasional frontal systems that generally approach from the northwest. The pier structure extends 330 m from shore in the west northwest direction. Water depth at the end of the pier is approximately 10 m. The end of the pier extends roughly 100 m past seaward of breaking waves. Meteorological sensors and air inlets were mounted at the end of a moveable 6 m boom mounted on the northwest corner of the pier. The boom was positioned to extend approximately into the prevailing winds. The sensing regions of the eddy covariance flux package and the air intake for chemical measurements were located approximately 10 m above the sea surface. Instrumentation for sulfur dioxide detection, data acquisition, clean air generator, and pumps were located in a trailer located at the end of the pier. Three-dimensional winds and fast response temperature measurements were measured using a Campbell CSAT 3 sonic anemometer, with data collection at 50 Hz. Water vapor and air density were measured using an open-path infrared gas analyzer (IRGA; LICOR model LI-7500) at 5 Hz. The instrument was calibrated using a dew point generator (LICOR model LI-610). Sea surface temperature was measured using a temperature probe array mounted on the pier with 9 probes vertically spaced by about 1 m. The sea surface temperature was taken to be the shallowest probe not exposed to air. Mean air temperatures were obtained from the NOAA meteorological station at the end of the pier.

For SO_2 detection, the air sampling inlet was similar to that used by Bell et al. (2013) to measure DMS. The air inlet was a 0.25" OD PFA tee fitting mounted just behind the sonic anemometer sensing region. Air was drawn into the inlet at a flow rate of 8500 cc min^{-1} and dried by passage through two counter-flow Nafion membrane driers (Perma Pure Inc. model PD-625-24PP) connected in series just after the inlet. The air passed from the driers through a 0.25" OD, 13 m long PFA Teflon tube to a chemical ionization mass spectrometer located in the trailer. In the trailer, 1000 cc min^{-1} of the 8500 cc min^{-1} air flow was drawn through the ionization source of the mass spectrometer. A 200 cc min^{-1} stream of ozonized dry air (Pen Ray UV lamp) was added to the 1000 cc min^{-1} prior to entry into the ionization source. A continuous flow of isotopically labeled gas standard ($^{34}SO_2$ in N_2) was injected into the sampled air stream at the inlet tee. This gas standard was delivered to the inlet

from an aluminum high pressure cylinder located in the trailer, at a flow rate ranging from 1-10 cc min^{-1} from a 1/8" O.D. PFA tube.

All flow rates were controlled and logged using mass flow controllers interfaced to a PC. Air for the Nafion counter-flow driers and ozone generator were supplied by a pure air generator and compressor (Aadco model 737-11), located in the trailer.

5 Pumping for the air inlet and ionization source was provided by a carbon vane pump (Gast model 1023)

3.2 SO$_2$ detection by chemical ionization mass spectrometry

Atmospheric SO$_2$ was detected using a laboratory-built chemical ionization mass spectrometer (CIMS) in negative ion mode. This instrument was described previously for positive ion measurements of dimethylsulfide (Bell et al., 2013). The instrument was modified for this study by replacing a set of conical declustering lenses with a multi-lens ion funnel of the design developed

10 by Kelly et al. (2010). This resulted in an order of magnitude improvement in ion transmission over the prior configuration of the instrument. In the CIMS instrument, ionization was carried out in a 0.25" inch glass lined stainless steel flow tube containing a ^{63}Ni foil at 430 Torr and room temperature, with an air flow rate of 1000 cc min^{-1}. Ions from the source enter the declustering region containing the ion funnel through a 250μ m diameter pinhole. The ion funnel is 127 mm long and consists of 100 concentric rings decreasing in diameter from 25.4 mm to 1.5 mm (Kelly et al., 2010). A DC gradient of 3 V cm^{-1} was

15 applied to transmit ions axially and two phases of RF (2MHz, 150V p-p) were applied so that adjacent rings in the funnel were 180°out of phase. The ion funnel was operated at a pressure of 1 Torr. Ions exit the ion funnel via a 1 mm orifice into the first stage of a differentially pumped Extrel quadrupole mass filter (19mm). Ions are detected using a dynode, ion multiplier, pulse amplifier/discriminator, and counting electronics (National Instruments model USB 6343). Ion counts were logged locally by the mass spectrometer control software and retransmitted as analog signals in real time with a fixed 2 second delay. The

20 analog signals were logged by the multichannel data logger along with data from the meteorological sensors. Sulfur dioxide was detected in negative ion mode as SO$_5^-$ (m/z 112), which was generated using the following reaction scheme previously described by (Thornton et al., 2002).

$$O_2^- + O_3 \rightarrow O_3^- + O_2 \tag{R5}$$

25 $$O_3^- + CO_2 \rightarrow CO_3^- + O_2 \tag{R6}$$

$$CO_3^- + SO_2 \rightarrow SO_3^- + CO_2 \tag{R7}$$

$$SO_3^- + O_2 + N_2 \rightarrow SO_5^- + N_2 \tag{R8}$$

Atmospheric
Chemistry
and Physics
Discussions
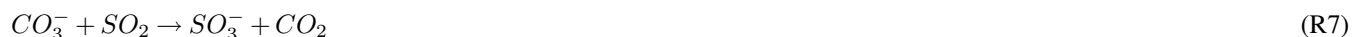
The addition of ozone minimizes the competing reaction $O_2^- + SO_2 \rightarrow SO_4^-$, and increases response to SO_2 (Möhler et al., 1992). When operating the ionization source at atmospheric pressure there was interference at m/z 112 from the $CO_4(H_2O)_2^-$ cluster ion. This was essentially eliminated by dropping the pressure in the source to 430 Torr.

Isotopically labeled $^{34}SO_2$ delivered to the air inlet served as an internal standard to account for any wall losses or variations in instrument sensitivity due to changes in ambient conditions. The flow rate of the gas standard was adjusted to achieve a $^{34}SO_2$ level of roughly 100 pmol mol^{-1} after dilution into the ambient air flow. The gas standard was prepared in our laboratory in a high-pressure aluminum gas cylinder (Scott Marin model 30A) and delivered via mass flow controller. These gas standards were calibrated in the lab against a gravimetrically calibrated permeation device using an inert dilution system described by Gallagher et al. (1997). The isotopically labelled standard was detected at m/z 114. The ambient SO_2 mixing ratio was calculated from the field data as follows:

$$X_{SO2} = \frac{S_{112}}{S_{114}} * \frac{F_{std}}{F_{total}} * X_{tank} \tag{9}$$

where S_{112} and S_{114} are the mass spectrometer signals (corrected for system blanks and for minor contamination of the $^{34}SO_2$ isotope-labelled standard with $^{32}SO_2$). F_{std} and F_{total} are the gas flow rates of the isotopic standard and inlet and X_{tank} is the molar mixing ratio of $^{34}SO_2$ in the compressed cylinder. Because the air stream was dried in the inlet tube prior to analysis, X_{SO2} represents the mixing ratio of SO_2 in dry air.

3.3 Flux data acquisition, post-processing, and gas transfer calculations

The analog data streams from the meteorological and chemical sensors were filtered with a Butterworth filter and logged at 50 Hz using a National Instruments multichannel data logger. Post-processing consisted of: 1) aligning the data to account for instrumental electronic delays and the delay due to the air flow transit time through the inlet tube, 2) rotating the 3-D winds for each flux interval into the frame of reference of the mean winds, 3) converting the data to geophysical units, 4) computing vertical fluxes of water vapor, sensible heat, SO_2 and momentum, 5) applying a high frequency correction to the SO_2 fluxes to account for loss of fluctuations in the inlet tubing, and 6) applying various quality control criteria to filter the resulting data set for instrumental issues or unsuitable environmental conditions. Data processing was carried out using Matlab (Mathworks). The inlet delay for SO_2 was determined experimentally in the laboratory prior to field deployments to be roughly one second. The measured delay was consistent with the offset required to maximizing the covariance between vertical wind and SO_2 concentration. Sulfur dioxide was measured as a dry mixing ratio since the air stream was dried prior to entering the mass spectrometer and converted to concentration (mol m^{-3}) using the dry air density. Water vapor concentrations measured by the LICOR were converted to mixing ratio (mol mol^{-1}). The saturation vapor pressure of seawater at the sea surface temperature was calculated following Sharqawy et al. (2010). Measured wind speeds were converted to 10 m winds for neutral atmospheric conditions (referred to hereafter as U_{10}) using the COARE algorithm (Fairall et al., 2000). The data set was subdivided into 13-minute flux intervals for processing. The resulting data consisted of means and variances for air temperature, relative humidity, SO_2, and seawater surface temperature. Fluxes of momentum, water vapor and SO_2 were calculated for each interval according

Atmospheric
Chemistry
and Physics
Discussions

to:

$$F_{SO2} = \overline{w'C'_{SO2}} \tag{10}$$

$$F_{H2O} = \overline{\rho}\,\overline{w'X'_{H2O}} \tag{11}$$

$$F_{mom} = \overline{\rho}\,\overline{w'U'} \tag{12}$$

$$F_{SH} = \overline{\rho}\,c_p\,\overline{w'T'} \tag{13}$$

w is the vertical wind and the primed quantities represent fluctuations about the mean, c_p is the heat capacity of air, and ρ is air density in kg m^{-3}, and the other variables are defined previously. Transfer velocities were computed following equations 1 and 3, as follows:

$$k_{SO2} = \frac{F_{SO2}}{C_{SO2}} \tag{14}$$

$$k_{H2O} = \frac{F_{H2O}}{(X_{H2O} - \overline{X_s})\,\overline{\rho_{dry}}} \tag{15}$$

$$k_{mom} = \frac{F_{mom}}{U_{10}\,\overline{\rho}} \tag{16}$$

$$k_{SH} = \frac{F_{SH}}{(\overline{T} - \overline{T_s})\,\overline{\rho}\,\overline{c_p}} \tag{17}$$

X_s is the calculated mixing ratio of water vapor corresponding to the saturation vapor pressure of water at the sea surface temperature.

3.4 High frequency correction for inlet tubing

High frequency fluctuations in the mixing ratio of SO$_2$ are attenuated during the passage of ambient air through inlet tubing and membrane driers. The attenuation characteristics of the inlet used in this study were characterized in the laboratory. This was done by delivering SO$_2$ to the CIMS instrument in an air stream at flow rates identical to those used in the field, and periodically interrupting the SO$_2$ flow. The resulting decay curves were fit to a 1st order low-pass Butterworth filter with a

cut-off frequency of 1.5 Hz. A high frequency correction factor or gain, G, was computed for each flux interval by applying the filter to the sonic temperature time series data and taking the ratio of the filtered and unfiltered fluxes as follows:

$$G = F_{\text{unfiltered}} / F_{\text{filtered}} \tag{18}$$

Linear regression of the gain against wind speed yielded $G=0.005U_{10}+1.018$. The SO_2 flux for each interval was multiplied by
5   the gain using this relationship and the mean wind speed for the interval.

3.5   Quality control criteria

Several quality control criteria were applied to the data to identify and eliminate flux intervals collected under unsuitable conditions or with instrumental problems. These were:

    1. Cospectral shape - A cumulative sum of cospectral density, normalized to the total flux, was computed for each flux
10   interval, summing from low to high frequency. Intervals were rejected if: a) the cumulative sum at 0.004 Hz exceeded the total flux or was opposite in sign, or b) the difference between cumulative flux at two consecutive frequencies exceeded 18%. These criteria identified most intervals with obvious deviations in co-spectral shape from those defined in Kaimal et al. (1972). Such intervals were largely caused by electronic noise on the sonic anemometer signal.

    2. Small air/sea differences - Intervals with air/sea concentration differences close to the propagated uncertainty of the
15   analytical measurements were eliminated. The criteria for water vapor, sensible heat, and SO_2 were 10^{-3} mol mol^{-1}, 0.7°C, 10 pmol mol^{-1}.

    3. Wind sector - Only intervals with onshore mean wind directions were used.

    4. Stable atmospheric conditions - Intervals with an atmospheric stability parameter, z/L, > 0.07 were rejected.

    5. Local SO_2 contamination - Intervals with sharp excursions in SO_2 associated with local contamination due to nearby
20   vessels were rejected.

4   Observations

4.1   Metorological and oceanic conditions

The field study was carried out from April 6-27, 2014. Time series of meteorological and oceanographic parameters and fluxes measured during this study are given in Fig. 1. Winds were generally light during the study, with a mean wind speed of 3.8±
25   2.0 m s^{-1} and a range of 0-9.7 m s^{-1}. Air temperatures were 16.2±1.3 °C with a range from 12.9-19.9 °C and the average relative humidity was 80%. Sea surface temperatures averaged 16.5±0.9 C with a range of 13.8-18.3 C. The SO_2 mixing ratio ranged from below detection to 560 pmol mol^{-1} with a mean of 100±114 pmol mol^{-1}. Sharp spikes in SO_2 were usually associated with military or commercial vessels passing upwind of the pier. Low SO_2 levels were associated with the occurrence of morning fog. For the first few days of the study, a high-pressure region was located over the study site (DOY 97-100) during
30   which winds were light and air temperatures were warm. Air mass back trajectories from this period indicate that marine air masses flowed from the north, passing inland over California before reaching the site. SO_2 levels were relatively high during

this time likely due to fossil fuel combustion. After the high-pressure system moved out of the region, air flow was from the northwest, arriving at the study site directly from the ocean and SO_2 levels were relatively low during this period. There was a notable increase in wind speed starting at DOY 106. On DOY 115 a low-pressure system passed over the region with higher wind speeds.

5　　The Scripps pier site experiences a consistent diurnal sea-breeze, with offshore flow during the evening and extending to the early morning. Data from periods with offshore flow were excluded from the analysis in the quality control process. Due to the sea-breeze locally and along the coast, there is likely advection of polluted air offshore, and the SO_2 levels measured during onshore flow may be elevated compared to marine air from the open ocean. The average air/sea temperature differential during the study was 0.56 ± 1.55 °C with a range from -3.5 to 2.7 °C with positive values indicating a warmer ocean than

10　atmosphere. Occasionally air/sea temperature differentials exhibited diurnal variability which reflected the changes in air temperatures. Starting around DOY 114 sea water temperatures warmed and were significantly warmer than air temperatures for the remaining three days of the study.

4.2　Air/sea differences and fluxes

All the observed SO_2 fluxes were from the atmosphere to the ocean surface (negative by convention) and ranged from 0 to -65

15　pmol m^{-2} s^{-1} with the largest fluxes observed at the beginning and end of the deployment associated with high SO_2 levels and high wind speeds respectively (Fig. 1). All observed water vapor and sensible heat fluxes passing quality control were upward which was consistent with the positive (from the ocean to the atmosphere) thermodynamic gradient for the duration of the study. The warm sea water temperatures combined with the high winds and cold temperatures on the last two days of the study resulted in large H_2O and heat fluxes.

20　　Frequency-weighted co-spectra of vertical wind and SO_2 are shown in Fig. 2. Fluxes measured during DOY 114-117 were significantly larger than those measured during the rest of the campaign because of the strong winds and large air/sea temperature differences observed during that period (Fig. 1). The co-spectra measured at Scripps Pier for all parameters were similar in shape to the characteristic boundary layer co-spectral shapes defined by Kaimal et al. (1972).

4.3　Transfer velocities

25　The wind speed dependence of k$_{mom}$ observed in this study was significantly greater than predicted using the open ocean parameterization from NOAA-COARE (Fairall et al., 2000) (Fig. 3). The relationship between wind speed and surface roughness can vary significantly between the open ocean and coastal environments because of bottom-generated turbulence, and other influences related to fetch, tidal currents, surfactants, and wave properties (Smith, 1988; Brown et al., 2013; Geernaert et al., 1986). Thus, the turbulent properties of the atmospheric surface layer in coastal environments are not well described by wind

30　speed alone. To account for such effects, we examined the relationship between transfer velocities and both wind speed and friction velocity (u$_*$) (Fig. 4).

　　The transfer velocities measured for water vapor, sensible heat and SO_2 (k$_{H2O}$, k$_{SH}$, k$_{SO2}$) were all positively correlated with friction velocity (Fig. 4, Table 1). k$_{mom}$ was signficantly larger than the scalar parameters and k$_{SO2}$ was smaller than

Atmospheric
Chemistry
and Physics
Discussions

k_{H2O} and k_{SH}. The regressions against friction velocity utilize slightly different data sets in each case because these regressions utilize flux measurement intervals that passed quality control for both the scalar parameter (water vapor, sensible heat, SO_2) and for momentum flux. This limits the amount of data available and means that the data sets used for the various parameters were not identical either in terms of the number of flux intervals or the physical conditions under which they were collected, i.e.

5 temperature, wind speed, atmospheric stability, sea state, etc.. Ideally, the comparison of transfer velocities would be carried out using intervals for which all four of the parameters passed quality control. However, given the limited data set this constraint reduced the available data to an unacceptable degree. As an alternative, we compared the data by computing two-way linear regressions between pairs of simultaneously measured transfer velocities (Figure 5, Table 2). This analysis was in agreement with the k vs u_* analysis described earlier and showed $k_{SO2} < k_{H2O}$, $k_{SO2} < k_{SH}$ and no significant difference between k_{SH}

10 and k_{H2O}. Momentum transfer velocities were significantly larger than all the scalar transfer velocities. The comparison of transfer velocities from simultaneous intervals is a more robust approach to observing differences in transfer velocities.

5   Discussion

This study demonstrates the successful measurement of SO_2 deposition to the sea surface using eddy covariance, with 1) cospectra exhibiting similar shape to water vapor and sensible heat and 2) a linear relationship between transfer velocities and

15 wind speed or friction velocity. Virtually all of the SO_2 cospectra indicated that the direction of flux was from air to sea, even during periods of very low atmospheric SO_2. This confirms the assumption that seawater SO_2 concentrations are highly undersaturated with respect to atmospheric SO_2. In general, we expect measurements of k_{SO2} to be of higher precision than those of water vapor and sensible heat because: 1) the SO_2 in seawater is negligible, so the air/sea concentration gradient is equal to the bulk atmospheric concentration, eliminating the need for a water side measurement, and 2) the SO_2 flux and atmospheric

20 concentration are determined simultaneously using a single sensor with a linear response, so the absolute calibration of the sensor does not influence the measured gas transfer velocity. These are advantages compared to the measurement of transfer velocities for water vapor or sensible heat, which require both air side and water side measurements in order to quantify the air/sea concentration or temperature difference.

One of the goals of this study was to compare observations of air-side controlled gas transfer velocities to parameterizations

25 in current use, such as COAREG (Fairall et al., 2000). The COAREG routine utilizes the open ocean COARE parameterization of friction velocity, based on wind speed and stability. As a result, COAREG substantially underestimates the observed transfer velocities for this nearshore coastal site. As noted earlier, momentum transfer coefficients at Scripps pier were elevated compared to those typically encountered under open ocean conditions. COAREG yields much better agreement with the field data when drag coefficients based on the measured friction velocities were substituted for those computed by COARE (Fig. 4). In this mode, the COAREG model is in good agreement with k_{H2O} and k_{SO2}. The model slightly underestimates k_{SH}. In

30 this study, the momentum transfer velocity was significantly (roughly 50%) larger than the transfer velocities of SO_2, water vapor, and sensible heat observed under simultaneous or similar conditions. This is reasonable, given that momentum can be

Atmospheric
Chemistry
and Physics
Discussions

transferred across the air/sea interface via both viscous stress (analogous to diffusion of mass or heat) and by pressure forces for which there is no analog in mass transfer.

Gas transfer coefficients should exhibit dependence on molecular diffusivity because of the role of molecular diffusion in the viscous layer adjacent to the sea surface. For air-side controlled gas transfer, a significant fraction of the overall resistance is due to turbulent transfer outside the interfacial layer. This component of the resistance should not exhibit dependence on molecular diffusion. In order to quantify the influence of molecular diffusion on the air-side of the interface, the diffusive component of the total resistance to gas transfer was estimated as:

$$r_{diffusion} = r_{total} - r_{turbulence} \tag{19}$$

where r_{total} for each gas is estimated from the inverse of the regression slopes of transfer velocities against u_*:

$$r_{total} = \frac{u_*}{k_{gas}} \tag{20}$$

Assuming that the air/sea transfer of momentum is primarily limited by turbulent transfer through the surface layer, we estimate turbulent resistance from the analogous slope for momentum:

$$r_{turbulence} = \frac{u_*}{k_{momentum}} \tag{21}$$

The diffusion-dependence of gas transfer was estimated from the relationships:

$$\frac{r_{diffH_2O}}{r_{diffSO_2}} = (\frac{Sc_{H_2O}}{Sc_{SO_2}})^n \qquad \frac{r_{diffSH}}{r_{diffSO_2}} = (\frac{Sc_{SH}}{Sc_{SO_2}})^n \tag{22}$$

using the turbulent and diffusive resistances determined for the Scripps field data and given in Table 3. Sc numbers for SO_2, and water vapor were calculated according to Fuller et al. (1966) using data provided by Reid et al. (1987) and the Sc number for sensible heat was calculated from Hilsenrath (1960) (Table 3). The molecular diffusivity of SO_2 is roughly half that of water vapor or sensible heat. Based on the Scripps pier data, we obtain estimates of n=0.79±1.3 for SO_2-water vapor and 0.51±1.8 for SO_2-sensible heat.

Diffusive resistance has been observed in the laboratory for water-side controlled gases, but has not been quantified for air-side gases under oceanic field conditions. Jähne et al. (1987) observed values of n in the range of 0.50 to 0.66 observed in the laboratory for smooth and rough flow conditions. Given the scatter in this rather limited dataset, the result is reasonably consistent with the range of 0.50 to 0.66 found by Jähne et al. (1987), suggesting that this approach may prove useful in characterizing the transport characteristics of the air side of the air/sea interface under field conditions.

6 Conclusions

This study demonstrated successful measurement of atmospheric deposition of SO_2 to the sea surface by eddy covariance. The high effective solubility and negligible seawater concentrations make SO_2 a useful tracer for studying the processes controlling air-side resistance to air/sea gas transfer. The deposition velocities found in this study are in reasonable agreement

Atmospheric
Chemistry
and Physics
Discussions

with bulk parameterizations in current use. This capability provides an opportunity to compare the transfer rates of air-side controlled substances with significantly different molecular diffusivities. The data from this study show that sulfur dioxide transfer velocities are smaller than those of momentum and water vapor, in agreement with gas transfer theory. This study was limited in terms of both the amount of data collected and the range of environmental conditions sampled. Further studies

5 conducted on the open ocean, covering a wider range of wind speeds, sea state, and air/water temperature differences could make a significant contribution to our understanding of the role of molecular diffusion in mass transfer between the atmosphere and ocean.

Code availability. TEXT

Data availability. TEXT

10 *Code and data availability.* TEXT

Sample availability. TEXT

Competing interests. There are no competing interests related to this manuscript

Atmospheric
Chemistry
and Physics
Discussions

Open Access

References

Bandy, A. R., Scott, D. L., Blomquist, B. W., Chen, S. M., and Thornton, D. C.: Low yields of SO_2 from dimethyl sulfide oxidation in the marine boundary layer, Geophysical Research Letters, 19, 1125–1127, https://doi.org/10.1029/92GL01041, http://dx.doi.org/10.1029/92GL01041, 1992.

5 Bandy, A. R., Thornton, D. C., Tu, F. H., Blomquist, B. W., Nadler, W., Mitchell, G. M., and Lenschow, D. H.: Determination of the vertical flux of dimethyl sulfide by eddy correlation and atmospheric pressure ionization mass spectrometry (APIMS), Journal of Geophysical Research: Atmospheres, 107, ACH 3–1–ACH 3–9, https://doi.org/10.1029/2002JD002472, http://dx.doi.org/10.1029/2002JD002472, 4743, 2002.

Bell, T. G., De Bruyn, W., Miller, S. D., Ward, B., Christensen, K. H., and Saltzman, E. S.: Air-sea dimethylsulfide (DMS) gas transfer in the
10 North Atlantic: evidence for limited interfacial gas exchange at high wind speed, Atmospheric Chemistry and Physics, 13, 11 073–11 087, https://doi.org/10.5194/acp-13-11073-2013, 2013.

Bowles, M. W., Mogollón, J. M., Kasten, S., Zabel, M., and Hinrichs, K.-U.: Global rates of marine sulfate reduction and implications for sub–sea-floor metabolic activities, Science, https://doi.org/10.1126/science.1249213, 2014.

Brown, J. M., Amoudry, L. O., Mercier, F. M., and Souza, A. J.: Intercomparison of the Charnock and COARE bulk wind stress formulations
15 for coastal ocean modelling, Ocean Science, 9, 721–729, https://doi.org/10.5194/os-9-721-2013, 2013.

Chin, M., Rood, R. B., Lin, S.-J., Müller, J.-F., and Thompson, A. M.: Atmospheric sulfur cycle simulated in the global model GOCART: Model description and global properties, Journal of Geophysical Research: Atmospheres, 105, 24 671–24 687, https://doi.org/10.1029/2000JD900384, 2000.

Cutter, G. and Krahforst, C.: Sulfide in surface waters of the western Atlantic Ocean, Geophysical Research Letters, 15, 1393–1396,
20 https://doi.org/10.1029/GL015i012p01393, cited By 63, 1988.

Danckwerts, P. V.: Significance of liquid-film coefficients in gas absorption, Industrial & Engineering Chemistry, 43, 1460–1467, https://doi.org/10.1021/ie50498a055, 1951.

De Bruyn, W. J., Dahl, E., and Saltzman, E. S.: DMS and SO_2 measurements in the tropical marine boundary layer, Journal of Atmospheric Chemistry, 53, 145–154, https://doi.org/10.1007/s10874-005-9000-z, 2006.

25 Elliott, S., Lu, E., and Rowland, F. S.: Carbonyl sulfide hydrolysis as a source of hydrogen sulfide in open ocean seawater, Geophysical Research Letters, 14, 131–134, https://doi.org/10.1029/GL014i002p00131, 1987.

Fairall, C. W., Hare, J. E., Edson, J. B., and McGillis, W.: Parameterization and micrometeorological measurement of air-sea gas transfer, Boundary-Layer Meteorology, 96, 63–106, https://doi.org/10.1023/A:1002662826020, 2000.

Faloona, I., Conley, S. A., Blomquist, B., Clarke, A. D., Kapustin, V., Howell, S., Lenschow, D. H., and Bandy, A. R.: Sulfur dioxide in the
30 tropical marine boundary layer: dry deposition and heterogeneous oxidation observed during the Pacific Atmospheric Sulfur Experiment, Journal of Atmospheric Chemistry, 63, 13–32, https://doi.org/10.1007/s10874-010-9155-0, 2009.

Fuller, E. N., Schettler, P. D., and Giddings, J. C.: New method for prediction of binary gas-phase diffusion coefficients, Industrial & Engineering Chemistry, 58, 18–27, https://doi.org/10.1021/ie50677a007, 1966.

Gallagher, M. S., King, D. B., Whung, P.-Y., and Saltzman, E. S.: Performance of the HPLC/fluorescence SO_2 detector dur-
35 ing the GASIE instrument intercomparison experiment, Journal of Geophysical Research: Atmospheres, 102, 16 247–16 254, https://doi.org/10.1029/97JD00700, 1997.

Geernaert, G. L., Katsaros, K. B., and Richter, K.: Variation of the drag coefficient and its dependence on sea state, Journal of Geophysical Research: Oceans, 91, 7667–7679, https://doi.org/10.1029/JC091iC06p07667, 1986.

Higbie, R.: The rate of absorption of a pure gas into a still liquid during short periods of exposure, Trans. AIChE, 31, 365–389, 1935.

Hilsenrath, J.: Tables of thermodynamic and transport properties of air, argon, carbon dioxide, carbon monoxide, hydrogen, nitrogen, oxygen, 5   and steam, Pergamon Press, 1960.

Hoover, T. E. and Berkshire, D. C.: Effects of hydration on carbon dioxide exchange across an air-water interface, Journal of Geophysical Research, 74, 456–464, https://doi.org/10.1029/JB074i002p00456, 1969.

Jähne, B., Münnich, K. O., Bösinger, R., Dutzi, A., Huber, W., and Libner, P.: On the parameters influencing air-water gas exchange, Journal of Geophysical Research: Oceans, 92, 1937–1949, https://doi.org/10.1029/JC092iC02p01937, 1987.

10   Kaimal, J. C., Wyngaard, J. C., Izumi, Y., and Coté, O. R.: Spectral characteristics of surface-layer turbulence, Quarterly Journal of the Royal Meteorological Society, 98, 563–589, https://doi.org/10.1002/qj.49709841707, 1972.

Kelly, R. T., Tolmachev, A. V., Page, J. S., Tang, K., and Smith, R. D.: The ion funnel: Theory, implementations, and applications, Mass Spectrometry Reviews, 29, 294–312, https://doi.org/10.1002/mas.20232, 2010.

Liss, P.: Exchange of SO_2 between the atmosphere and natural waters, Nature, 233, 327, https://doi.org/doi:10.1038/233327a0, 1971.

15   Liss, P.: Processes of gas exchange across an air-water interface, in: Deep Sea Research and Oceanographic Abstracts, vol. 20, pp. 221–238, Elsevier, 1973.

Liss, P. and G. Slater, P.: Flux of Gases Across the Air-Sea Interface, 247, 181–184, 1974.

Liu, W. T., Katsaros, K. B., and Businger, J. A.: Bulk parameterization of air-sea exchanges of heat and water vapor including the molecular constraints at the interface, Journal of the Atmospheric Sciences, 36, 1722–1735, https://doi.org/10.1175/1520-
20   0469(1979)036<1722:BPOASE>2.0.CO;2, 1979.

Mackay, D. and Yeun, A. T. K.: Mass transfer coefficient correlations for volatilization of organic solutes from water, Environmental Science & Technology, 17, 211–217, https://doi.org/10.1021/es00110a006, pMID: 22304636, 1983.

Millero, F. J., Hershey, J. B., Johnson, G., and Zhang, J.-Z.: The solubility of SO_2 and the dissociation of H_2SO_3 in NaCl solutions, Journal of Atmospheric Chemistry, 8, 377–389, https://doi.org/https://doi.org/10.1007/BF00052711, 1989.

25   Möhler, O., Reiner, T., and Arnold, F.: The formation of SO5- by gas phase ion-molecule reactions, The Journal of Chemical Physics, 97, 8233–8239, https://doi.org/10.1063/1.463394, 1992.

Radford-Knoery, J. and Cutter, G. A.: Biogeochemistry of dissolved hydrogen sulfide species and carbonyl sulfide in the western North Atlantic Ocean, Geochimica et Cosmochimica Acta, 58, 5421 – 5431, https://doi.org/https://doi.org/10.1016/0016-7037(94)90239-9, 1994.

Reid, R. C., Prausnitz, J. M., and Poling, B. E.: The properties of gases of liquids: Their estimation and correlation. 4th Ed., McGraw-Hill, 30   1987.

Schwartz, S. and Freiberg, J.: Mass-transport limitation to the rate of reaction of gases in liquid droplets: Application to oxidation of SO_2 in aqueous solutions, Atmospheric Environment, 15, 1129 – 1144, https://doi.org/https://doi.org/10.1016/0004-6981(81)90303-6, 1981.

Sharqawy, M. H., V, J. H. L., and Zubair, S. M.: Thermophysical properties of seawater: a review of existing correlations and data, Desalination and Water Treatment, 16, 354–380, https://doi.org/10.5004/dwt.2010.1079, 2010.

35   Sheng, J.-X., Weisenstein, D. K., Luo, B.-P., Rozanov, E., Stenke, A., Anet, J., Bingemer, H., and Peter, T.: Global atmospheric sulfur budget under volcanically quiescent conditions: Aerosol-chemistry-climate model predictions and validation, Journal of Geophysical Research: Atmospheres, 120, 256–276, https://doi.org/10.1002/2014JD021985, 2014JD021985, 2015.

Slinn, W., Hasse, L., Hicks, B., Hogan, A., Lal, D., Liss, P., Munnich, K., Sehmel, G., and Vittori, O.: Some aspects of the transfer of atmospheric trace constituents past the air-sea interface, Atmospheric Environment (1967), 12, 2055 – 2087, https://doi.org/https://doi.org/10.1016/0004-6981(78)90163-4, 1978.

Smith, S. D.: Coefficients for sea surface wind stress, heat flux, and wind profiles as a function of wind speed and temperature, Journal of

5   Geophysical Research: Oceans, 93, 15 467–15 472, https://doi.org/10.1029/JC093iC12p15467, 1988.

Thornton, D. C., Bandy, A. R., Tu, F. H., Blomquist, B. W., Mitchell, G. M., Nadler, W., and Lenschow, D. H.: Fast airborne sulfur dioxide measurements by Atmospheric Pressure Ionization Mass Spectrometry (APIMS), Journal of Geophysical Research: Atmospheres, 107, ACH 13–1–ACH 13–10, https://doi.org/10.1029/2002JD002289, 4632, 2002.

Worsnop, D. R., Zahniser, M. S., Kolb, C. E., Gardner, J. A., Watson, L. R., Van Doren, J. M., Jayne, J. T., and Davidovits, P.: The temperature

10 dependence of mass accommodation of sulfur dioxide and hydrogen peroxide on aqueous surfaces, The Journal of Physical Chemistry, 93, 1159–1172, https://doi.org/10.1021/j100340a027, 1989.

Zhang, J.-Z. and Millero, F. J.: The rate of sulfite oxidation in seawater, Geochimica et Cosmochimica Acta, 55, 677 – 685, https://doi.org/https://doi.org/10.1016/0016-7037(91)90333-Z, 1991.

Atmospheric
Chemistry
and Physics
Discussions

Table 1. Two-way regression of transfer velocities against friction velocity (k/u_*).

Parameter	Regression slope (cm m^{-1}) $\pm$ 1 s.e.	Number of observations
Water vapor (k_{H2O}/u_*)	3.33±0.65	67
Sensible heat (k_{SH}/u_*)	3.06±0.93	37
Sulfur dioxide (k_{SO2}/u_*)	2.74±0.62	22
Momentum (k_{mom}/u_*)	4.79±0.37	85

Table 2. Pair-wise regression of transfer velocities using simultaneously measured data from Figs. 3 and 4.

Parameter	Regression slope $\pm$ 1 s.e.	Number of data points
Sulfur dioxide vs. water vapor (k_{SO2} vs. k_{H2O})	0.63$\pm$0.14	33
Sulfur dioxide vs. sensible heat (k_{SO2} vs. k_{SH})	0.57$\pm$0.15	21
Water vapor vs. sensible heat(k_{H2O} vs k_{SH})	0.91$\pm$0.15	69
Sulfur dioxide vs. momentum (k_{SO2} vs k_{mom})	0.54$\pm$0.26	22
Water vapor vs. momentum (k_{H2O} vs k_{mom})	0.71$\pm$0.15	67
Sensible heat vs. momentum (k_{SH} vs k_{mom})	0.76$\pm$0.15	37

Table 3. Resistance to gas transfer separated into total, turbulent and diffusive terms. Diffusion coefficients and Schmidt numbers are also given, as calculated according to Fuller et al. (1966) and Hilsenrath (1960).

Parameters	H_2O	Sensible heat	SO_2
Total resistance (r_{total})	30.0±5.9	32.7±9.9	35.5±8.3
Turbulent resistance ($r_{turbulent}$)	20.9±1.6	20.9±1.6	20.9±1.6
Diffusive resistance ($r_{diffusive}$)	9.2±6.1	11.8±10.0	15.6±8.4
Diffusion coefficient in air (298 K; cm^2 s^{-1})	0.25	0.22	0.13
Sc number (Sc; 298 K)	0.61	0.69	1.19

Atmospheric
Chemistry
and Physics
Discussions
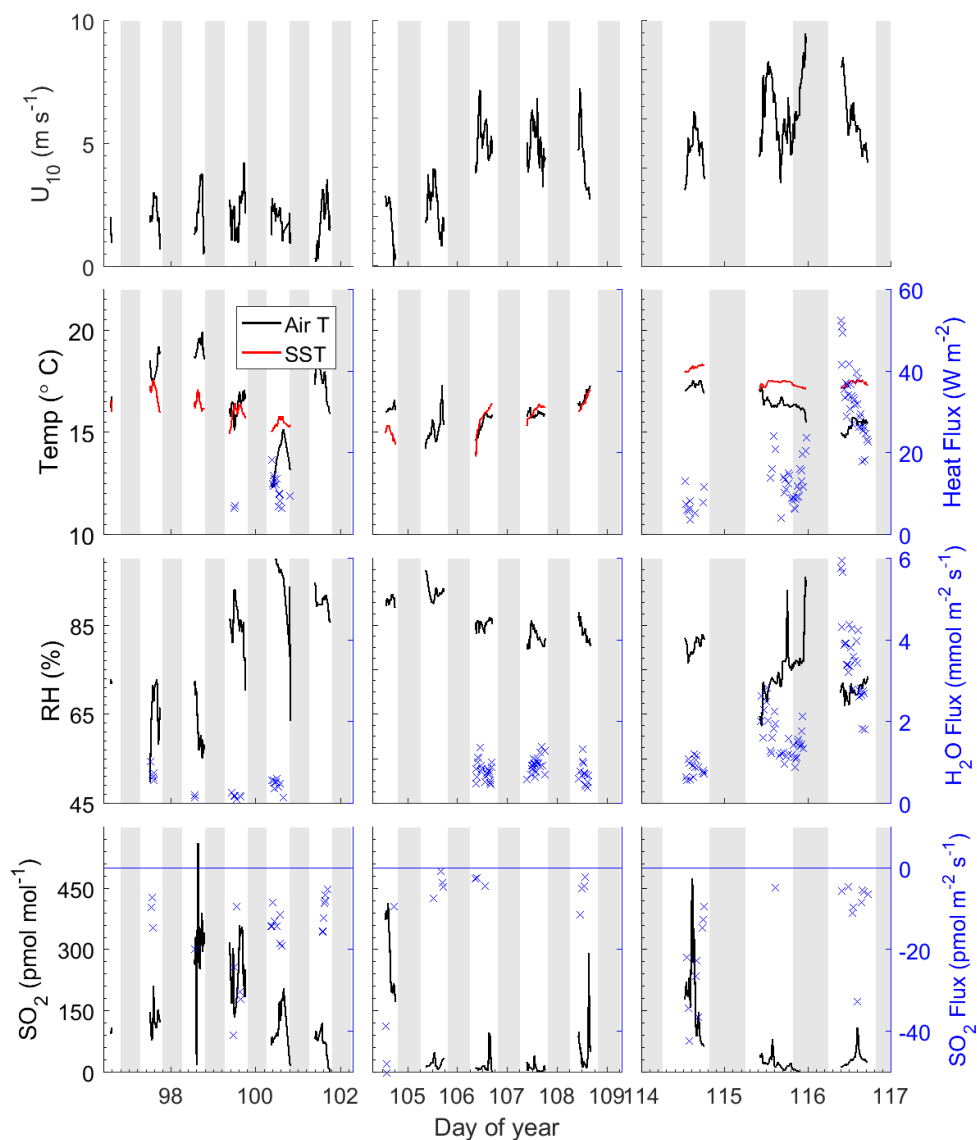
Figure 1. Time series of meteorological and oceanographic parameters measured on Scripps pier during April 6-27, 2014. The grey bands indicate night. The blue symbols (x, right y-axis) are fluxes that passed quality control.

Atmospheric
Chemistry
and Physics
Discussions
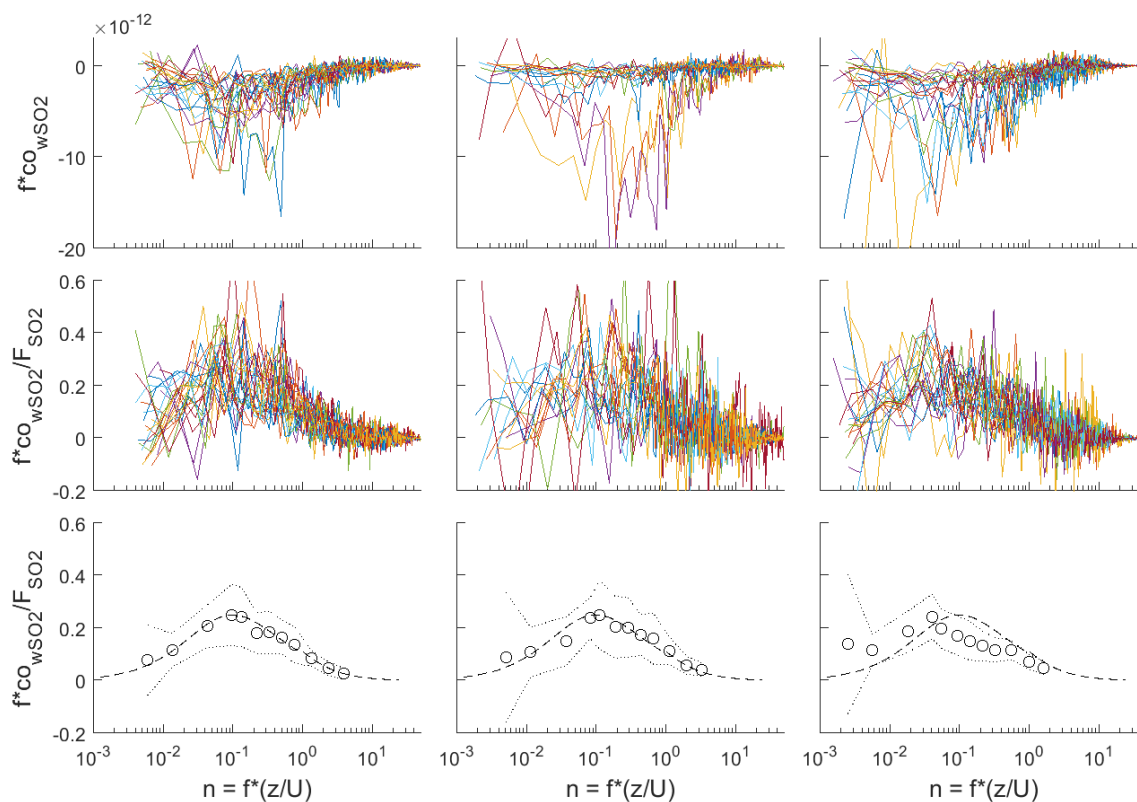
Figure 2. Frequency weighted cospectra of vertical wind and SO₂ concentration for flux intervals collected at Scripps Pier during three time periods. Left column: DOY 96-102; Center column: DOY 104-109; Right column: DOY 114-117. Top row: individual co-spectra for 13-minute flux intervals; Middle row: Same as top except co-spectra have been normalized to the average flux during the interval. Bottom row: Bin-averages of the flux normalized co-spectra (circles), ± 1 standard deviation (dotted line), and idealized cospectral shape from Kaimal et al. (1972) (dashed line).
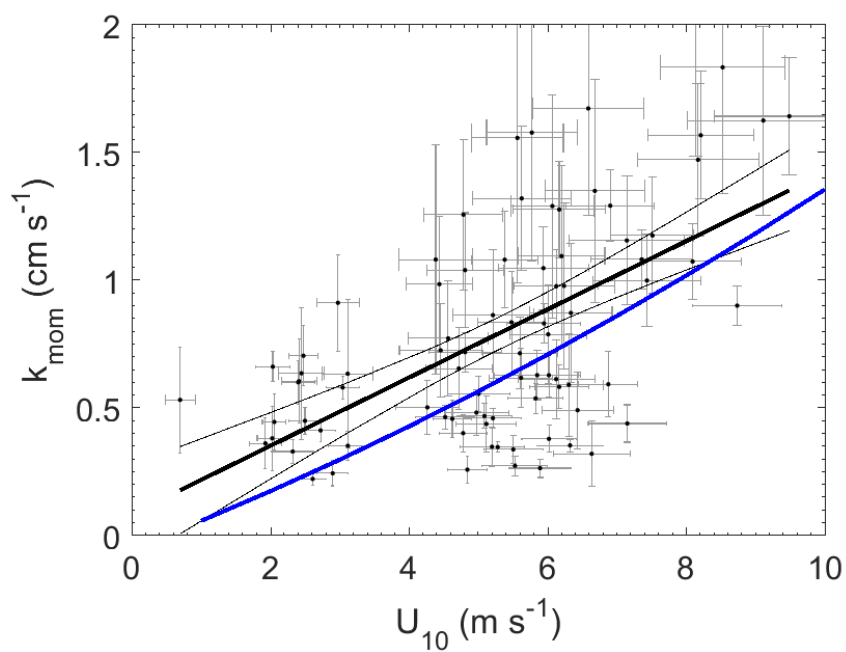
Figure 3. Momentum transfer velocities measured at Scripps Pier as a function of wind speed with linear least squares regression and 95% confidence intervals (black). Blue line - COAREG parameterization of Fairall et al. (2000).
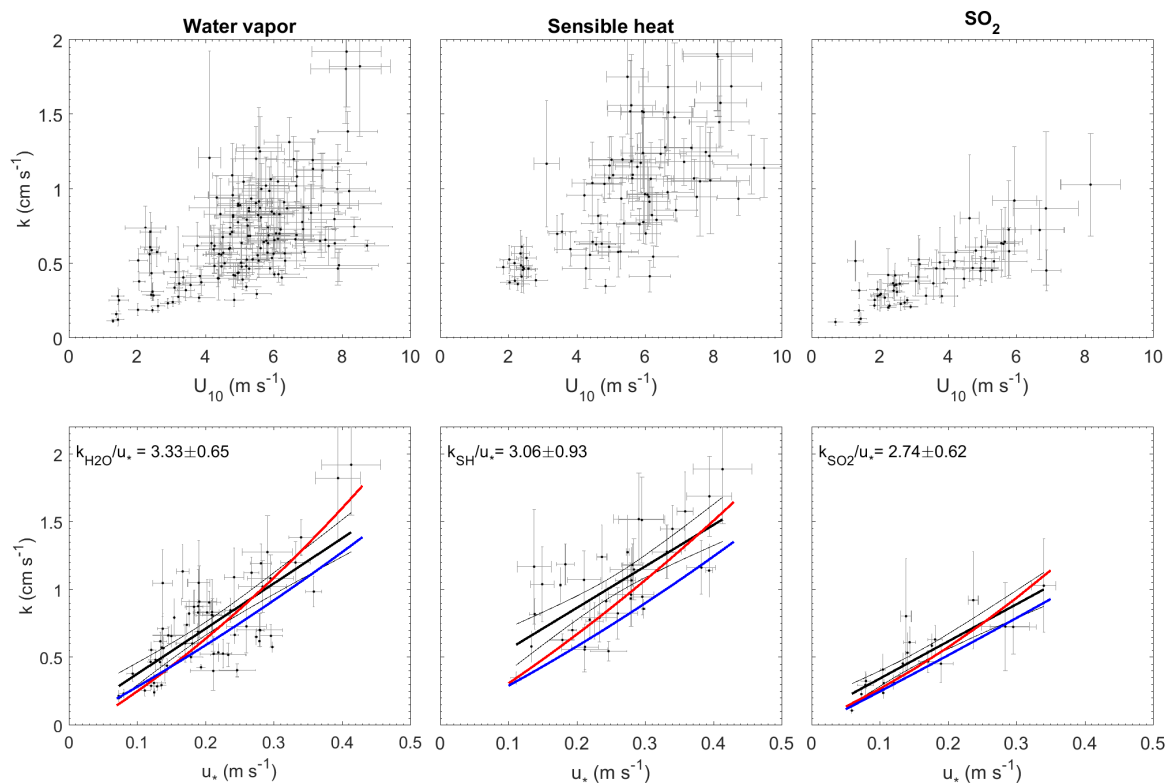
Figure 4. Transfer velocities measured at Scripps Pier as a function of wind and friction velocity. Top row: water vapor, sensible heat, and SO_2 as a function of U_{10}. Bottom row: water vapor, sensible heat, and SO_2 as a function of u_* with linear least squares regressions and 95% confidence intervals (black). Red lines are the COAREG parameterization of Fairall et al. (2000) using friction velocities and drag coefficients from the Scripps field measurements. Blue lines - COAREG parameterization using friction velocities and drag coefficients computer by the model.

Atmospheric
Chemistry
and Physics
Discussions
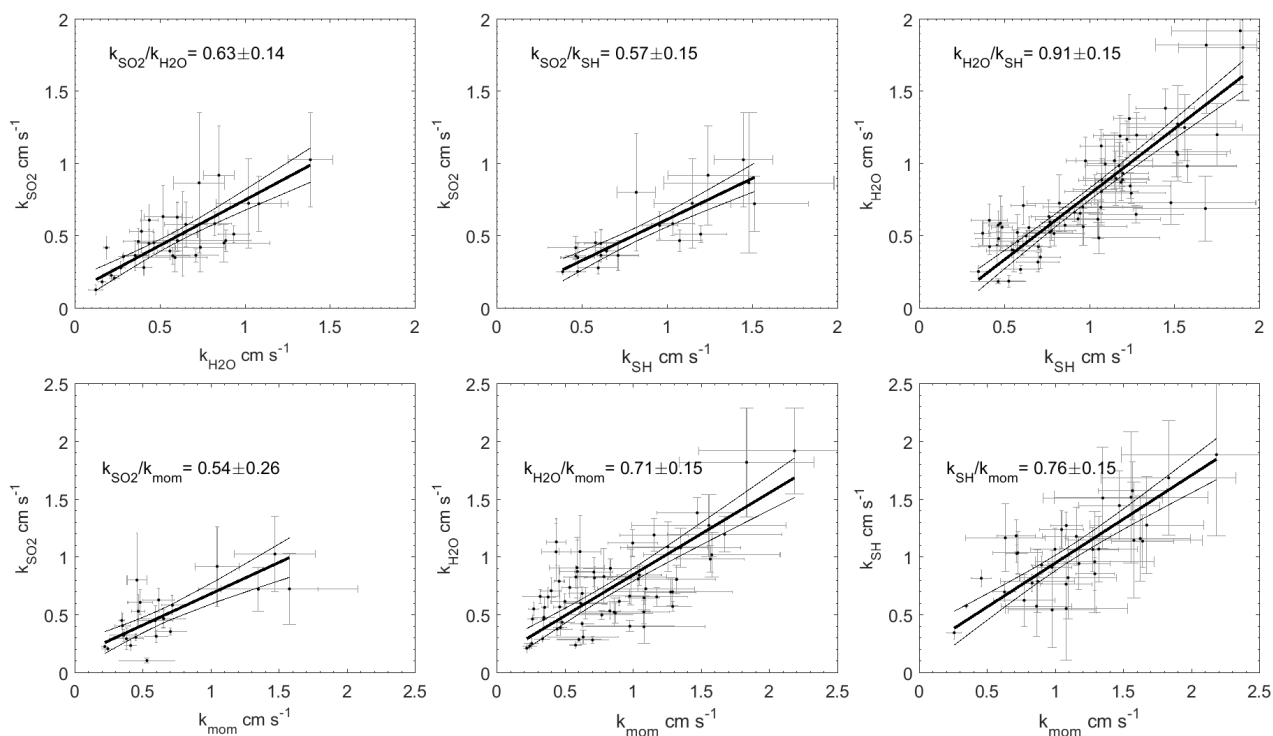
Figure 5. Two-way regressions of transfer velocities measured at Scripps Pier. Top row: water vapor, sensible heat, SO$_2$ against each other.

Bottom row: SO$_2$, water vapor, and sensible heat regressed against momentum. 95% confidence intervals are shown.